A novel hardware-efficient CPG model based on asynchronous coupling of cellular automaton phase oscillators for a hexapod robot

Kentaro Takeda
Graduate School of Science and Engineering
Hosei University
Tokyo, Japan
E-mail: takeda@mail.nsci.jp

Hiroyuki Torikai
Graduate School of Science and Engineering
Hosei University
Tokyo, Japan
E-mail: torikai@hosei.ac.jp

***Abstract*—In this paper, a novel hardware-efficient central pattern generator (CPG) model based on asynchronous coupling of cellular automaton (CA) phase oscillators for a hexapod robot is presented. It is shown that the presented model can exhibit various synchronization patterns depending on parameter values. In order to analyze the synchronization patterns, a phase equilibrium and an evaluation function for a target synchronization pattern are introduced. As a result of the analysis, it is shown that an asynchronously coupled CA phase oscillators is suitable for the hexapod robot than a synchronously coupled CA phase oscillators. The presented asynchronous CPG model with parameters tuned appropriately is implemented on a field programmable gate array (FPGA) device and the device is mounted on a hexapod robot. A laboratory experiment verifies that the hexapod robot can reproduce one of typical gaits of six-legged insects. Finally, it is shown that the presented CPG model consumes far fewer circuits elements and much less power compared with one of conventional numerical integration CPG model and our previous CPG model.**

***Index Terms*—Central Pattern Generator (CPG), Nonlinear dynamics, Synchronization, Hexapod Robot, Asynchronous Cellular Automaton, Field Programmable Gate Array (FPGA)**

I. Introduction

Multi-legged creatures perform various kinds of locomotions by periodic motions of flexor and extensor muscles driven with coordinated body movements. It has been widely accepted for several decades that the periodic motions are produced by central pattern generators (CPGs), which consist of groups of neurons located in central nervous systems [1]. There has been an increasing an interest in artificial robots inspired by the biological principle such as CPGs that can carry out useful tasks in various environments [2]. For controlling artificial robots, many models of CPGs have been proposed so far [2]–[24], where typical ones are modeled as coupled neural oscillators described by ordinary differential equations, e.g., Hopf oscillators [11] and its phase-reduced versions, Kuramoto oscillators [16]. From a view point of the nonlinear dynamical system theory, the neuromorphic models including CPG models are classified into the following four classes based on continuousness and discontinuousness of state variables and times[1].

This work is partially supported by KAKENHI grant number 19J20745 and 18K11482.

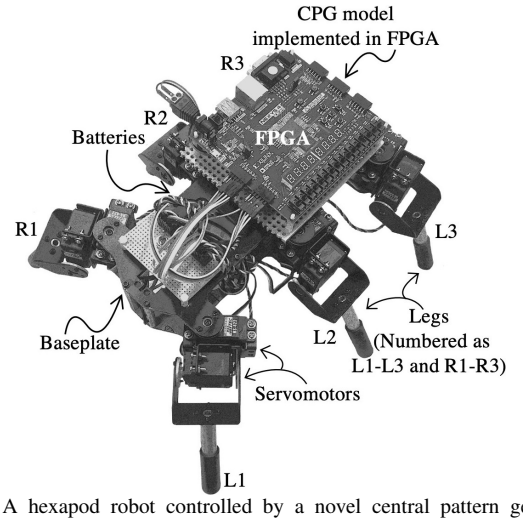

Fig. 1. A hexapod robot controlled by a novel central pattern generator (CPG) model based on ring-coupled asynchronous cellular automaton (CA) phase oscillators implemented in a field programmable gate array (FPGA). The robot body and the servomotors are based on Lynxmotion's MH2 hexapod robot [27].

Class CTCS: A nonlinear differential equation model of a neuromorphic system having *a continuous time and continuous states* (CTCS). Such a class CTCS neuromorphic model can be typically implemented by an analog nonlinear circuit, e.g., [3]–[10].

Class DTDS: A numerical integration model (in finite binary number representations) of a neuromorphic system having *a discrete time and discrete states* (DTDS). Such a class DTDS neuromorphic model can be typically implemented by a digital processor or a sequential logic circuit, e.g., [11]–[17].

Class DTCS: A nonlinear difference equation model of a neuromorphic system having *a discrete time and continuous states* (DTCS). Such a class DTCS neuromorphic model can be typically implemented by a switched capacitor circuit, e.g., [18]–[21].

[1]Partial differential equation models are omitted for simplicity.

978-1-7281-6926-2/20/$31.00 ©2020 IEEE

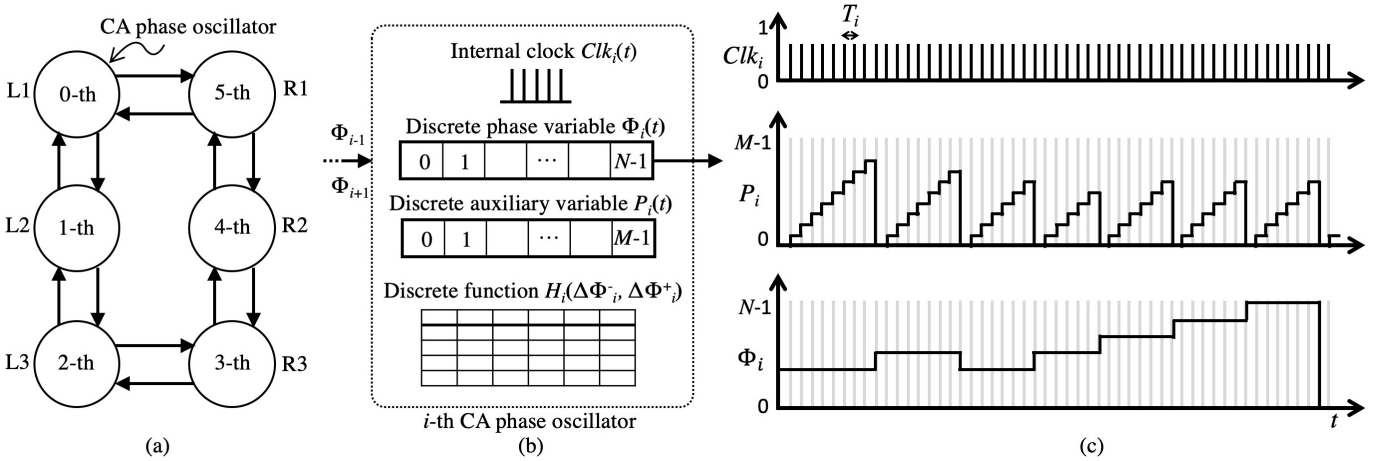

Fig. 2. (a) Coupling diagram of the central pattern generator (CPG) model consisting of the cellular automaton (CA) phase oscillators. (b) Schematic diagram of the i-th CA phase oscillator. (c) Timing chart of the i-th CA phase oscillator.

Class CTDS: An asynchronous cellular automaton model (CA) of a neuromorphic system having *a continuous (state transition) time and discrete states* (CTDS). Such a class CTDS neuromorphic model can be typically implemented by an asynchronous sequential logic circuit, e.g., [22]–[25].

It goes without saying that most neuromorphic models are belonging to the classes CTCS, DTDS, and DTCS. On the other hand, our group has been developing class CTDS neuromorphic models [22]–[25]. Also, our group has been demonstrating advantages of the class CTDS neuromorphic models, e.g., the models can be typically implemented by using much fewer circuit elements and consume much less power compared to class DTDS neuromorphic models [22]–[25]. Hence, this paper addresses the following issues: (i) proposal of a novel class CTDS CPG model for a hexapod robot, (ii) analysis of its nonlinear dynamics (e.g., comparison between synchronously coupled and asynchronously coupled phase oscillators), (iii) implementation the proposed model in a field programmable gate array (FPGA) mounted on a prototype hexapod robot, and (iv) comparisons with a typical conventional CPG model and our previous CPG model [24].

Contributions and novelties of this paper include the following points.

- The class CTDS CPG model can be implemented by using much fewer circuit elements and consumes much less power compared to both a class DTDS CPG model and the model presented by our previous paper [24]. Hence, the results of this paper will contribute to design small and low-power silicon CPG devices, where applications of which will include an implantable neural prosthesis device and an ultra-small controller for a micro robot.
- This paper presents a class CTDS CPG model based on coupled CA phase oscillators for the first time. Although our group presented a class CTDS CPG model to control a snake robot [22][23] and a hexapod robot [24], these models consist of non-phase-reduced nonlinear oscillators. By modeled with phase-reduced oscillators, the presented model has fewer variables than our previous models [22]–[25] and thereby circuit elements needed to implement on an FPGA can be further reduced as mentioned above.
- This paper analyzes the difference in behaviors between the synchronously coupled CA phase oscillators and the asynchronously coupled CA phase oscillators for the first time. As a result, it can be conclude that the asynchronously coupled CA phase oscillators are suitable for a CPG model. Hence, the results of this paper will be important elements of dynamical system theories (e.g., oscillation, synchronization, and bifurcation theories) of class CTDS neuromorphic systems.

II. CPG MODEL BASED ON ASYNCHRONOUS COUPLING OF CA PHASE OSCILLATOR

A. Model description

In this subsection, a novel CPG model based on asynchronous coupling of cellular automaton (CA) phase oscillators for a hexapod robot is presented. Fig. 1 shows a hexapod robot, which has a baseplate, twelve servomotors, six legs, batteries and a field programmable gate array (FPGA). Also, Fig. 2(a) shows a coupling diagram of the presented CPG model, which is implemented in the FPGA. As shown in this figure, the CPG model consists of the six CA phase oscillators, where the oscillators are numbered as L1–L3 and R1–R3 corresponding to the legs shown in Fig. 1. Fig. 2(b) shows a schematic of each CA phase oscillator. As shown in this figure, each CA phase oscillator has the following internal clock $Clk_i \in \{0, 1\}$.

Internal clock:

$$Clk_i(t) = \sum_{l=0}^{\infty} \delta(t - lT_i), \tag{1}$$

where $t \in \mathbf{R}$ is a continuous time; $i \in \{0, \cdots, n-1\}$ is an index for the CA phase oscillators in a ring topology defined by the periodic conditions, i.e., $Clk_n = Clk_0$ and $Clk_{n+1} =$

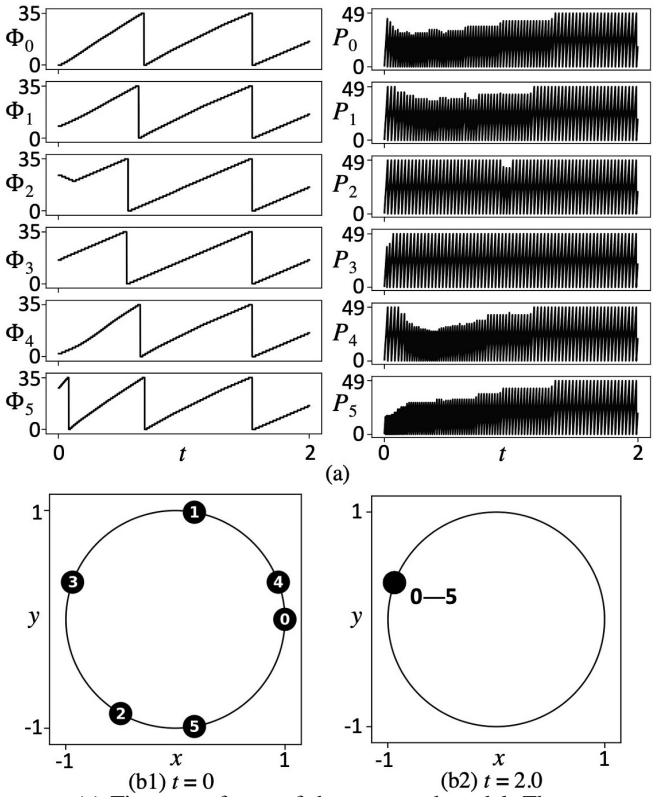

Fig. 3. (a) Time waveforms of the presented model. The parameters are $n = 6$, $N = 36$, $M = 50$, $\Gamma = 1$, $\omega_i = 1.0$, $F_{clk} = 1800$, and $f_0^{clk} = 1800$ for all i. The initial values are $P_i(0) = 0$ for all i, $\Phi_0(0) = 0$, $\Phi_1(0) = 8$, $\Phi_2(0) = 24$, $\Phi_3(0) = 16$, $\Phi_4(0) = 2$, and $\Phi_5(0) = 28$. (b) Cartesian coordinate representation of the unit circle. The i-th oscillator is plotted at $x = \cos(2\pi\Phi_i/N)$ and $y = \sin(2\pi\Phi_i/N)$ as the black circles with the numbers of the indexes. (b1) Initial states at $t = 0$. (b2) Steady states at $t = 2.0$.

Clk_1; $T_i \in (0, \infty)$ represents a period of the i-th internal clock Clk_i; and $\delta : \mathbf{R} \to \{0, 1\}$ is the following unit impulse

$$\delta(t) = \begin{cases} 1 & \text{if } t = 0, \\ 0 & \text{if } t \neq 0. \end{cases}$$

Each internal clock Clk_i triggers state transitions of discrete variables as shown in Fig. 2(c). Hence, the CA oscillators can be said to be

$$\begin{cases} \text{synchronously coupled} & \text{if } f_i^{clk}/f_j^{clk} = 1 \text{ for all } i \text{ and } j, \\ \text{asynchronously coupled} & \text{otherwise,} \end{cases} \tag{2}$$

where $f_i^{clk} = T_i^{-1}$ represents frequency of the i-th internal clock Clk_i. The difference in behaviors between the synchronously coupled oscillators and the asynchronously coupled CA phase oscillators is discussed in Subsection C. As shown in Fig. 2(b), each CA phase oscillator has the following discrete phase variable.

Discrete phase variable:

$$\Phi_i \in \mathbf{Z}_N = \{0, \cdots, N-1\}.$$

Each discrete phase variable controls the servomotor of the leg in the hexapod robot. Also, as shown in Fig. 2(b), each CA phase oscillator has the following discrete auxiliary variable.

Discrete auxiliary variable:

$$P_i \in \mathbf{Z}_M = \{0, \cdots, M-1\}.$$

Fig. 2(c) shows a timing chart of the clock Clk_i, P_i, and Φ_i for the i-th CA phase oscillator. As shown in this figure, each internal clock Clk_i triggers the following transition of the discrete auxiliary variable P_i.

Transition of the discrete auxiliary variable:

$$\text{If } Clk_i(t) = 1, \text{ then}$$
$$P_i(t_+) := \begin{cases} P_i(t) + 1 & \text{if } P_i(t) < |H_i(\Delta\Phi_i^-, \Delta\Phi_i^+)|, \\ 0 & \text{if } P_i(t) \geq |H_i(\Delta\Phi_i^-, \Delta\Phi_i^+)|, \end{cases} \tag{3}$$

where

$$\Delta\Phi_i^- \equiv \Phi_{i-1}(t) - \Phi_i(t) \text{ and } \Delta\Phi_i^+ \equiv \Phi_{i+1}(t) - \Phi_i(t)$$

denote the phase differences of the CA phase oscillators; "t_+" denotes "$\lim_{\varepsilon \to +0} t + \varepsilon$"; and the symbol ":=" denotes an "instantaneous state transition" throughout the paper. Also, the discrete function $H_i : \mathbf{Z}_N^{\pm} = \{-(N-1), \cdots, (N-1)\} \times \mathbf{Z}_N^{\pm} \to \mathbf{Z}_M^{\pm} = \{-(M-1), \cdots, (M-1)\}$ is defined as follows.

Discrete coupling function:

$$H_i(\Delta\Phi_i^-, \Delta\Phi_i^+) = \Big\lfloor \frac{F_{clk}}{N(\omega_i + \Gamma h(\Delta\Phi_i^-, \Delta\Phi_i^+))} \Big\rfloor, \tag{4}$$

where the function is assumed to be saturated at $\pm(M-1)$; $\Gamma \in \mathbf{R}$, $F_{clk} \in (0, \infty)$ and $\omega_i \in (0, \infty)$ represent a coupling constant, a scaling factor, and a natural angular frequency of each CA phase oscillator, respectively; and $\lfloor . \rfloor$ denotes the following floor function,

$$\lfloor x \rfloor = \max\{l \in \mathbf{Z} \mid l \leq x\}.$$

Also, the function $h : \mathbf{Z}_N^{\pm} \times \mathbf{Z}_N^{\pm} \to \mathbf{R}$ is defined as follows.

$$h(\Delta\Phi_i^-, \Delta\Phi_i^+) = \sin\Big(\frac{2\pi\Delta\Phi_i^-}{N}\Big) + \sin\Big(\frac{2\pi\Delta\Phi_i^+}{N}\Big). \tag{5}$$

Note that the discrete coupling function H_i is implemented on lookup tables. As shown in Fig. 2(c), each internal clock Clk_i triggers the following transition of the discrete phase variable Φ_i.

Transition of the coupling of the discrete phase variable:

$$\text{If } Clk_i(t) = 1 \text{ and } P_i(t) \geq |H_i(\Delta\Phi_i^-, \Delta\Phi_i^+)|, \text{ then}$$
$$\Phi_i(t_+) := \begin{cases} \Phi_i(t)+1 & \text{if } H_i(\Delta\Phi_i^-, \Delta\Phi_i^+) \geq 0 \text{ and } \Phi_i(t) < N-1, \\ 0 & \text{if } H_i(\Delta\Phi_i^-, \Delta\Phi_i^+) \geq 0 \text{ and } \Phi_i(t) = N-1, \\ \Phi_i(t)-1 & \text{if } H_i(\Delta\Phi_i^-, \Delta\Phi_i^+) < 0 \text{ and } \Phi_i(t) > 0, \\ N-1 & \text{if } H_i(\Delta\Phi_i^-, \Delta\Phi_i^+) < 0 \text{ and } \Phi_i(t) = 0. \end{cases} \tag{6}$$

Note that since the transition times of whole oscillators may have ergodicity in a case of the asynchronous coupling, it is necessary to be defined as a continuous time, that means the model is regarded to be belonging to the class CTDS system as described in Section I. Fig. 3(a) shows typical time waveforms of the coupled CA phase oscillators. Also, Figs. 3(b1) and (b2) show the Cartesian coordinate representations of the discrete

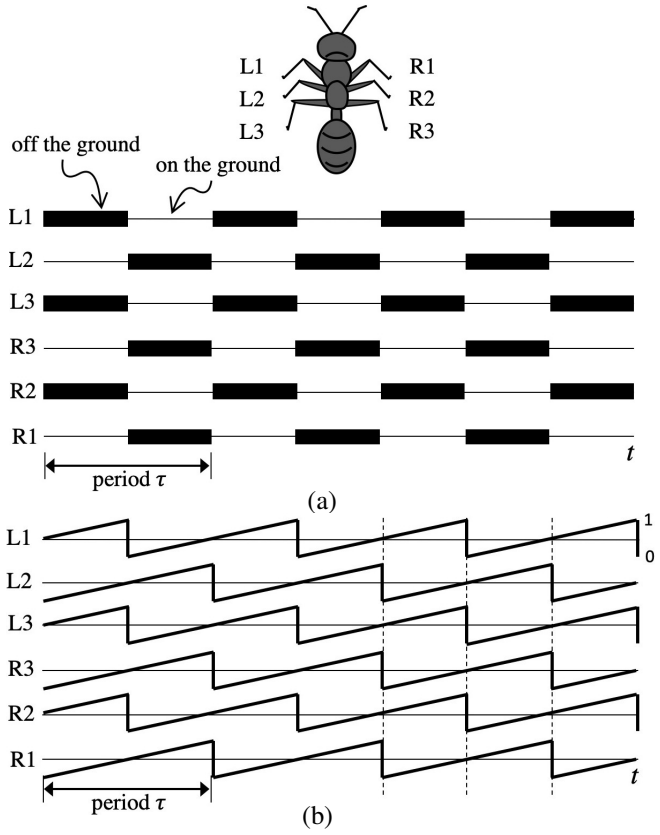

Fig. 4. (a) Illustration of the six-legged insect and gait diagram [26]. (b) Illustration of the target synchronization pattern described by the phase equation $\phi_i(t)$ corresponding to (a).

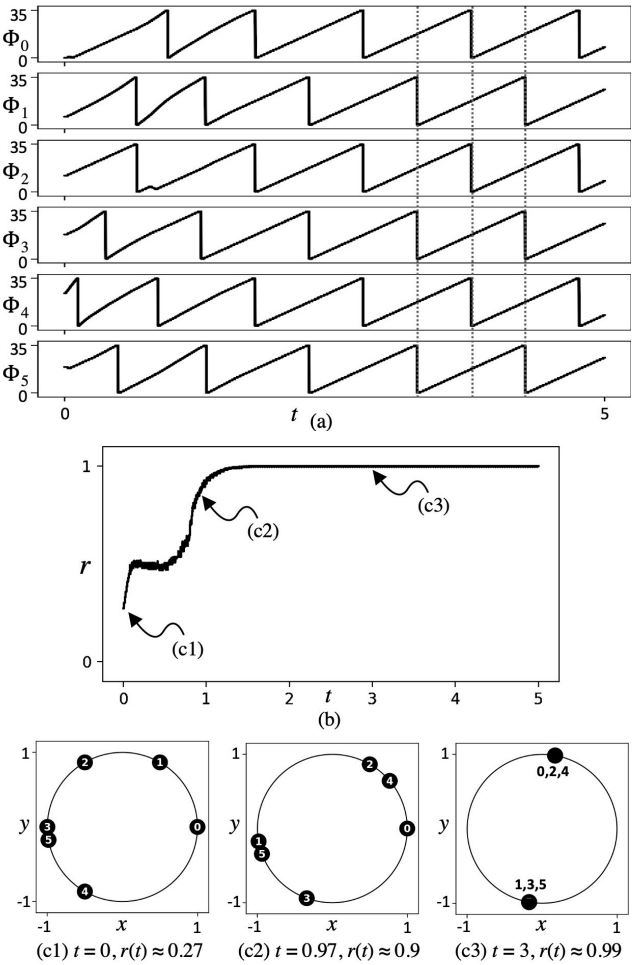

Fig. 5. (a) Time waveforms of the presented model. The values of the coupled CA phase oscillators are $n = 6$, $N = 36$, $M = 50$, $\Gamma = -1$, $F_{clk} = 1800$, $\omega_i = 1.0$, and $f_i^{clk} = 1800$ for all i. The values of the initial states are $P_i(0) = 0$ for all i, $\Phi_0(0) = 0$, $\Phi_1(0) = 6$, $\Phi_2(0) = 12$, $\Phi_3(0) = 18$, $\Phi_4(0) = 24$, and $\Phi_5(0) = 19$. (b) Instantaneous evaluation function for the target synchronization r with respect to time t. (c1–c3) Cartesian coordinate representations on the unit circle corresponding to the states indicated by the arrows in (b).

phase variables Φ_i the unit circles at $t = 0$ and $t = 2.0$. In this case, the coupled CA phase oscillators exhibit in-phase synchronization. Also, it is confirmed that the coupled CA phase oscillators exhibit various other synchronization states by changing initial conditions and coupling constant Γ. Then, the next subsection introduces a target synchronization pattern for the hexapod robot.

B. Target synchronization for the hexapod robot

Fig. 4(a) shows an illustration of an insect and a tripod gait diagram, which is one of typical gaits of six-legged insects [26]. As shown in the upper illustration of Fig. 4(a), the six legs are numbered as L1–3 and R1–3. In the lower diagram, the horizontal axis represents time and the vertical axis represents the movements of each leg relative to the ground. The black bars indicate the moments when each leg is off the ground and moving forward. In the white regions (i.e., the regions other than black bars), each leg is touching the ground. As indicated in Fig. 4(a), a pair of black bar and white region can be regarded as a gait pattern with period τ. As shown in Fig. 4(b), let us consider the following phase signal: $\phi_i(t) = \tau^{-1}t + \bar{\phi}_i \pmod 1$, where $\phi_i(t), \bar{\phi}_i \in [0, 1)$ and $i \in \{0, 1, \cdots, 5\}$. Let us also consider the following map: $\sigma(\phi_i(t)) =$ "white region" if $\phi_i(t) < 1/2$ and $\sigma(\phi_i(t)) =$ "black bar" otherwise. As shown in Figs. 4(a) and (b), the phase signal $\phi_i(t)$ can be converted into the gait diagram by the map σ. Hence, in this study, let the set of the phase signals $\{\phi_i(t)\}$ in Fig. 4(b) be the target pattern since the gait of a robot can be controlled by them. The features of the target synchronization pattern can be summarized as follows.

Target synchronization pattern:

1. The phase signals corresponding to legs (R1, L2, R3) exhibit in-phase synchronization.
2. The phase signals corresponding to legs (L1, R2, L3) exhibit in-phase synchronization.
3. The phase signals of the group of the legs (R1, L2, R3) and the oscillations of the group of the legs (L1, R2, L3) exhibit anti-phase synchronization.

In order to evaluate the synchronized states of the coupled CA phase oscillators, the following instantaneous evaluation function for the target synchronization pattern is introduced.

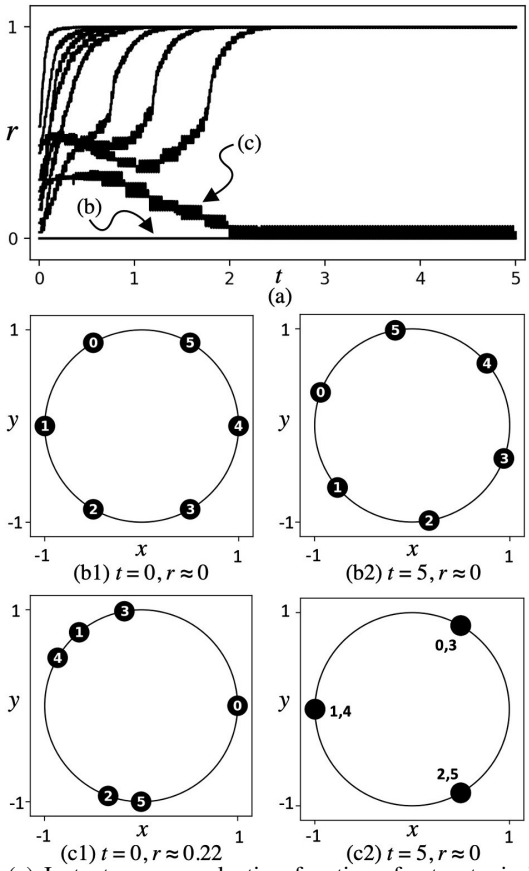

Fig. 6. (a) Instantaneous evaluation functions for ten typical initial states $(\Phi_i, \cdots, \Phi_{n-1})$. The values of the parameters are $n = 6$, $N = 36$, $M = 50$, $\Gamma = -1$, $\omega_i = 1.0$, and $f_i^{clk} = 1800$ for all i. The fixed values of the initial states are $P_i(0) = 0$ for all i. (b1–2) Cartesian coordinate representations at $t = 0$ and $t = 5$ corresponding to the states indicated by the arrow (b) in (a). The initial states are $\Phi_0(0) = 0$, $\Phi_1(0) = 13$, $\Phi_2(0) = 25$, $\Phi_3(0) = 10$, $\Phi_4(0) = 15$, and $\Phi_5(0) = 27$. (c1–2) Cartesian coordinate representations at $t = 0$ and $t = 5$ corresponding to the states indicated by the arrow (c) in (a). The initial states are $\Phi_0(0) = 4$, $\Phi_1(0) = 10$, $\Phi_2(0) = 16$, $\Phi_3(0) = 22$, $\Phi_4(0) = 28$, and $\Phi_5(0) = 34$.

Instantaneous evaluation function for the target synchronization pattern:

$$r(t) = \frac{1}{n}\left| \sum_{i=0}^{n/2-1} e^{\mathrm{j}2\pi\Phi_{2i}(t)/N} + e^{\mathrm{j}((2\pi\Phi_{2i+1}(t)/N)-\pi)} \right|, \quad (7)$$

where $0 \le r(t) \le 1$, $\mathrm{j} = \sqrt{-1}$, and the indexes i are mapped to the leg numbers in Fig. 4(a) as shown in Fig. 2(a).

The instantaneous evaluation function r close to 1 means the target synchronization pattern has been achieved. Fig. 5(a) shows time waveforms of the coupled CA phase oscillators for $\Gamma = -1$. The states of the discrete phase variables Φ_i at t indicated by the three dashed lines in Fig. 5(a) are consistent with ones indicated by the three dashed lines in Fig. 4(b). On the other hand, Fig. 5(b) shows the instantaneous evaluation function r with respect to t. Actually, it can be seen that the instantaneous function r is approaching 1 over time. In addition, Figs. 5(c1)–(c3) show the three cases of the discrete phase variables Φ_i on the Cartesian coordinates corresponding to ones indicated by the arrows (c1)–(c3) in Fig. 5(b). The features of the states of the discrete phase variables Φ_i in Fig. 5(c3) consistent with the three features of the target synchronization pattern. Hence, it can be said from the above that the coupled CA phase oscillators in Fig. 5 is achieving the target synchronization pattern. Here, let us see the following example of the instantaneous evaluation function r for various initial states of the discrete phase variables Φ_i.

Example (Failure to synchronize to target pattern): Fig. 6 shows the instantaneous evaluation function r with respect to t for ten typical initial states $(\Phi_0, \cdots, \Phi_{n-1})$. The other initial states are fixed as $P_i(0) = 0$ for all i. Also, each parameter f_i^{clk} and ω_i are respectively set to the same values for all i. Note that this parameter setting is considered to be appropriate from a view point of reducing hardware resources. In Fig. 6(a), the coupled CA phase oscillators for almost all initial states achieve the target synchronization pattern but two cases are failed. Figs. 6(b1–2) and (c1–2) show the states of the discrete phase variables Φ_i on the Cartesian coordinate of the two failed cases corresponding to the arrows (b) and (c) in Fig. 6(a). The consequent synchronized states in Figs. 6(b2) and (c2) differ from the features of the target synchronization state and its Cartesian coordinate representation in Fig. 5(c3).

The example suggests that the coupled CA oscillators have the target synchronization pattern and other synchronizations, which do not exhibit the target synchronization pattern. Here, let us clarify all the synchronization patterns that the coupled CA oscillators have. The vector forms of the discrete variables P_i, and Φ_i can be written by

$$\begin{aligned} \mathbf{P}(t) &= (P_0(t), \cdots, P_{n-1}(t)), \\ \mathbf{\Phi}(t) &= (\Phi_0(t), \cdots, \Phi_{n-1}(t)). \end{aligned} \quad (8)$$

In order to characterize an equilibrium in terms of synchronization, the following definition is introduced.

Definition 1 (Phase equilibrium state): *The coupled CA phase oscillators are said to be in a* phase equilibrium state *if the coupled CA phase oscillators satisfy the following conditions:*

1. *Each CA phase oscillator has the same value of the parameter ω_i, that is, $\omega_i = \omega_j$* for all i and j.
2. $\mathbf{P}(t) \in \mathbf{P}^*$ and $\mathbf{\Phi}(t) \in \mathbf{\Phi}^*$ for some t, *where*

$$\begin{aligned} \mathbf{P}^* &= \{(P_0, \cdots, P_{n-1}) \mid P_i = P_j \text{ for all } i \text{ and } j\}, \\ \mathbf{\Phi}^* &= \{(\Phi_0, \cdots, \Phi_{n-1}) \mid h(\Delta\Phi_i^-, \Delta\Phi_i^+) = 0 \text{ for all } i\}. \end{aligned} \quad (9)$$

Also, it is said that the coupled CA phase oscillators exhibit l-phase synchronization if the coupled CA phase oscillators are in a phase equilibrium state*, where*

$$l = \begin{cases} 1 & \text{if } \Phi_i^+ = 0, \\ \dfrac{N}{|\Phi_i^+|} & \text{if } \Phi_i^+ \neq 0. \end{cases}$$

Note that Definition 1 doesn't care whether a phase equilibrium is stable or unstable. Hence, the coupled CA phase oscillators are not necessarily phase-locked even if Definition

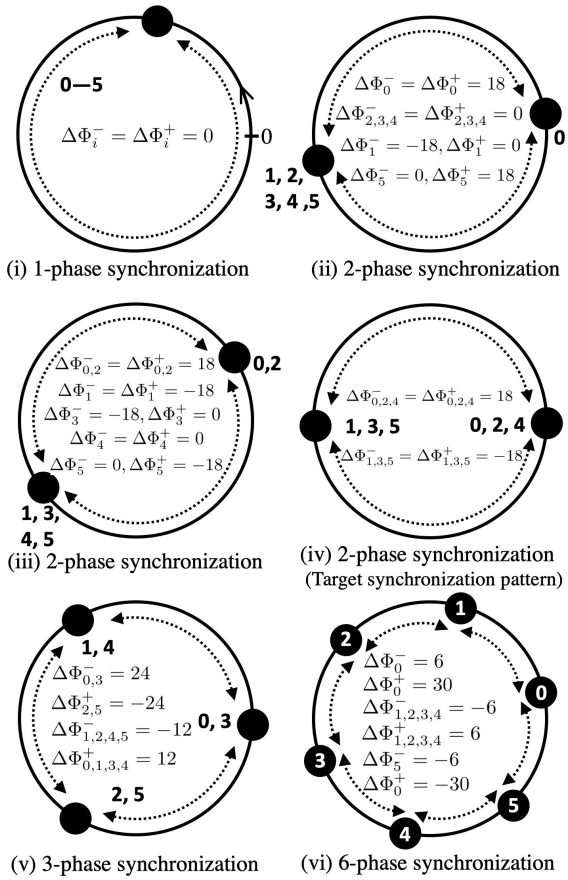

Fig. 7. Examples of the phase equilibrium states. There are $L = 4$ types of the l-phase synchronizations in the case of $n = 6$ and $N = 36$. (i) 1-phase synchronization. It is also called in-phase synchronization. (ii) 2-phase synchronization. (iii) 2-phase synchronization. (iv) 2-phase synchronization (Target synchronization pattern). (v) 3-phase synchronization. (vi) 6-phase synchronization.

1 is satisfied. Fig. 7 shows examples of the phase equilibrium states. As shown in this figure, there are L types of *l-phase synchronization* depending on the parameters N and n, where L can be estimated as follows.

$$L = \#\{m \in \mathbf{N} \mid N(\mathrm{mod}\ m) = 0 \text{ and } n(\mathrm{mod}\ m) = 0\}.$$

where $\#$ denotes the number of elements in a set. For example, as shown in Fig. 7, there are $L = 4$ types of the l $(= 1, 2, 3$ or $6)$-phase synchronization in the case of $n = 6$ and $N = 36$. Also, Definition 1 regards the target synchronization patten as the 2-phase synchronization. Using the instantaneous evaluation function $r(t)$ and Definition 1, the next subsection compares the synchronously coupled CA oscillators and the asynchronously coupled CA oscillators.

C. Comparison of synchronous and asynchronous coupling

First, let us see the following example of the instantaneous evaluation function r for initial states chosen from phase equilibrium states.

Case I (Synchronous coupling of CA phase oscillators): Fig. 8(a) shows the instantaneous evaluation function r with respect to t for six initial states chosen from the sets $\mathbf{\Phi}^*$ and

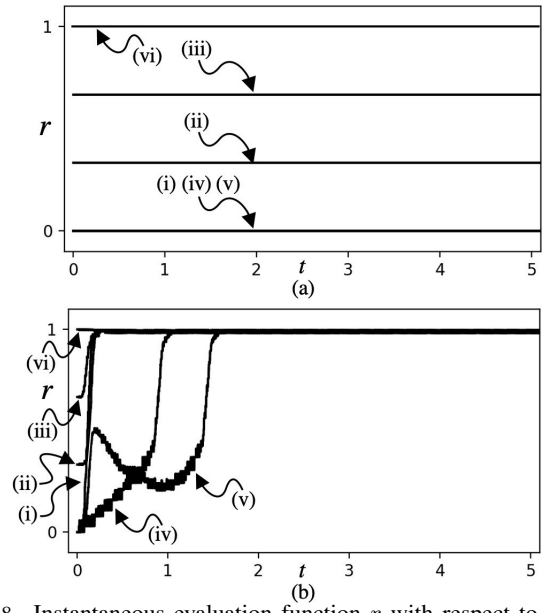

Fig. 8. Instantaneous evaluation function r with respect to t for six initial states $\mathbf{\Phi}(0) \in \mathbf{\Phi}^*$ and $\mathbf{P}(0) \in \mathbf{P}^*$ corresponding to (i)–(vi) in Fig. 7. The values of parameters are $n = 6$, $N = 36$, $M = 50$, and $\Gamma = -2$, $\omega_i = 1.0$ for all i. (a) Synchronous coupled CA phase oscillators. $f_i^{clk} = 1800$ for all i. (b) Asynchronously coupled CA phase oscillators. $f_0^{clk} = 1800$, $f_1^{clk} = 1800$, $f_2^{clk} = 1800$, $f_3^{clk} = 1800$, $f_4^{clk} = 1800$, and $f_i^{clk} = 2640$.

$\mathbf{P}^*$ corresponding to the six examples in Fig. 7. In this figure, the all cases fail to synchronize to the target synchronization pattern except for the case of the initial states corresponding to the target synchronization pattern itself (i.e., the arrow (vi) in Fig. 8(a)). In this example, the clock parameters f_i^{clk} are set to the same values for all i. Hence, the model is regarded as the synchronous coupling of the CA phase oscillators.

The reason why the coupled CA phase oscillators in Case I keep the initial states can be supposed as follows. When the CA phase oscillators satisfy Definition 1, the function H_i has the following constant value,

$$H_i(\Delta\Phi_i^-, \Delta\Phi_i^+) = \left\lfloor \frac{F_{clk}}{N\omega_i} \right\rfloor.$$

Hence, if Definition 1 is satisfied and the parameters f_i^{clk} are set to the same values for all i, the CA phase oscillators keep holding its l-phase synchronization states since the discrete state transitions defined by Eqs. (3) and (6) are always triggered at the same time. Then, let us see the following example of the instantaneous evaluation function r in the case of the asynchronous coupling of the CA phase oscillators.

Case II (Asynchronous coupling of CA phase oscillators): Fig. 8(b) shows the instantaneous evaluation function r with respect to t for six initial states chosen from the sets $\mathbf{\Phi}^*$ and $\mathbf{P}^*$ corresponding to the six examples in Fig. 7. In this example, the values of the clock parameters are $f_0^{clk} = 1800$, $f_1^{clk} = 1800$. $f_2^{clk} = 1800$, $f_3^{clk} = 1800$, $f_4^{clk} = 1800$, and $f_5^{clk} = 2640$. Hence, the model is regarded as the asynchronous coupling of the CA oscillators. As shown in Fig. 8(b), the all cases achieve the target synchronization pattern.

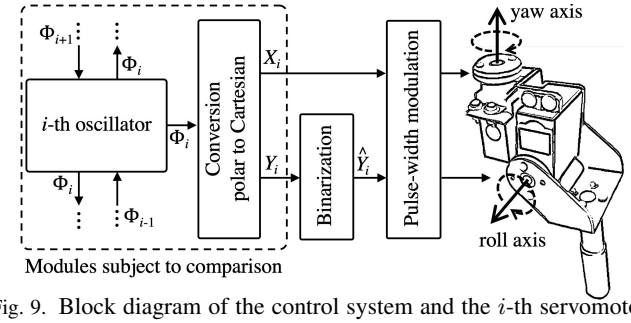

Fig. 9. Block diagram of the control system and the i-th servomotor.

The reason why the coupled CA phase oscillators in Case II can achieve the target synchronization pattern unlike Case I can be supposed as follows. When the values of the parameters f_i^{clk} differ by at least one, the asynchronously coupled CA phase oscillators can escape from a phase equilibrium state even if an initial condition is set to a phase equilibrium since there are times that n clocks do not trigger at the same time. Note that the oscillators that escapes from a phase equilibrium may reenter the phase equilibrium. As a result, the advantage of the asynchronous coupling of the CA oscillators can be summarized as follows.

Remark on advantage of asynchronous coupling: The coupled CA oscillators have generally some phase equilibria as shown in Fig. 7. However, it is not preferable that the CPG model has phase equilibrium states that exhibit synchronization patterns different from the target synchronization pattern as shown in Fig. 6(a). If the clock parameters are chosen so that the n oscillators transit asynchronously, it may be possible to synchronize to the target synchronization pattern for any initial states as shown in Fig. 8(b). Hence, it can be said that the asynchronous coupling of the CA oscillators is suitable for the CPG model for a hexapod robot.

III. Implementation and Comparison

A. Implementation

Fig. 9 shows the block diagram of a control system for the i-th leg, where each leg has the two servomotors corresponding to the 2-DOF. As shown in this figure, the discrete phase variable Φ_i is converted to a Cartesian coordinate representation from a polar coordinate representation as follows.

Conversion from polar to Cartesian:

$$X_i(t) = F(\Phi_i(t)),\ Y_i(t) = G(\Phi_i(t)),$$

where the discrete functions $F : \mathbf{Z}_N \to \mathbf{Z}$ and $G : \mathbf{Z}_N \to \mathbf{Z}$ are as follows.

$$F(\Phi) = \lfloor E\cos(2\pi\Phi/N)\rfloor,\ G(\Phi) = \lfloor E\sin(2\pi\Phi/N)\rfloor,$$

where E is a scaling parameter of resolution for pulse-width modulation. The discrete functions F and G are implemented on lookup tables. As shown in Fig. 9, the servomotors corresponding to yaw axes are controlled by pulse width-modulated signals of the discrete state variables X_i. Also, the servomotors corresponding to roll axes are controlled by pulse width-modulated signals of the following discrete variables binarized from the discrete variables Y_i.

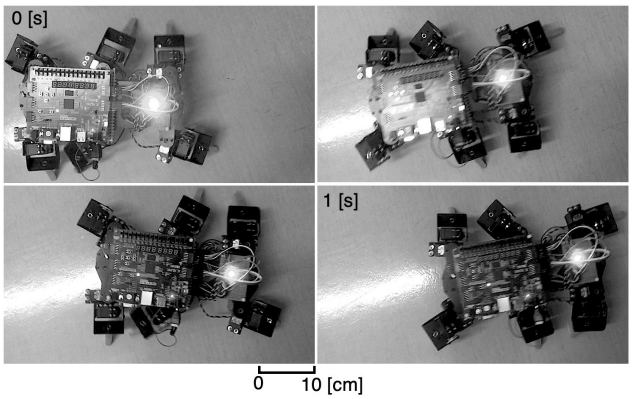

Fig. 10. Snapshots of locomotion of the hexapod robot.

Binarization:

$$\hat{Y}_i(t) = \begin{cases} A & \text{if } Y_i(t) \geq 0, \\ -A & \text{otherwise.} \end{cases}$$

Recall that the dynamics of the presented CPG model is described by Eqs. (3) and (6). These dynamics, the discrete states $\{\Phi_i, P_i, X_i, Y_i, \hat{Y}_i\}$, and the discrete functions $\{H_i, F, G\}$ are written as a VHDL code in a register-transfer level description. The code is compiled by Xilinx's design software environment Vivado 2018. 2 and a resulting bitstream file is downloaded to Xilinx's FPGA Artix-7 XC7A100T-1CSG324C [28] mounted on Digilent's Nexys 4 DDR evaluation platform [29]. Since the FPGA device does not support asynchronous triggering, the internal clocks Clk_i are generated from a common clock with a high frequency (100 [MHz]). Fig. 10 shows snapshots of locomotions of the hexapod robot controlled by the presented CPG model. The laboratory experiments confirmed that the hexapod robot can reproduce the tripod gait.

B. Comparison

The presented CPG model is compared with our previous CPG model [24] and the following Hopf CPG model [2], which is one of typical conventional CPG models.

Hopf CPG model[2]:

$$\begin{aligned} \frac{dx_i}{dt} &= F_x(x_i, y_i) + \sum_{j=0}^{n} w_{i,j}x_j, \\ \frac{dy_i}{dt} &= F_y(x_i, y_i) + \sum_{j=0}^{n} w_{i,j}y_j, \\ F_x(x_i, y_i) &= (\mu_i^2 - (x_i^2 + y_i^2))x_i - \theta_i y_i, \\ F_y(x_i, y_i) &= (\mu_i^2 - (x_i^2 + y_i^2))y_i + \theta_i x_i, \end{aligned} \tag{10}$$

where $n = 6$ is the number of oscillators, $x_i \in \mathbf{R}$ and $y_i \in \mathbf{R}$ are state variables controlling phases of the 2-DOF legs, and $w_{i,j}$ represents a coupling constant. In our previous paper [24], the Hopf CPG model has implemented by the forward Euler method on the same FPGA device and design software environment for comparison with our previous CPG model, where the bit-lengths of the state variables are shortened as short as possible under the condition that the robot can reproduce the tripod gait appropriately. Also, the robots controlled by the three types of CPG model can move forward at the almost

identical gait speed. The comparison result suggests that the presented CPG model can be implemented by about 59% of FPGA slices of our previous CPG model and about 14% of FPGA slices of the Hopf CPG model. Also, the presented CPG model consumes about 69% of total on-chip power of our previous CPG model and about 27% of total on-chip power of the Hopf CPG model.

IV. Conclusion

This paper presented the novel class CTDS CPG model based on the asynchronous coupling of the CA phase oscillators for the hexapod robot. The difference in behaviors between the synchronously coupled CA phase oscillators and the asynchronously coupled CA phase oscillators was analyzed. As a result, it was shown that the asynchronously coupled CA phase oscillators is suitable for the hexapod robot than the synchronously coupled CA phase oscillators. The laboratory experiments verified that the robot controlled by the presented CPG model reproduces the tripod gait. It was shown that the presented CPG model consumes much fewer circuit elements and much less power compared to the conventional model and our previous model. These results imply the presented model will contribute to develop an ultra-small and ultra low-power gait controller for a micro robot and an implantable neural controller for prosthesis of rehabilitation of gaits. In order to develop such gait controllers, the following problems remain: (a) validation of robustness for disturbances such as obstructions and slope changes by more experiments, (b) reproduction of many types of gaits, (c) realization of smooth gait transitions, gait velocity changes, and sudden braking, and (d) theoretical analyses of synchronization and bifurcation phenomena.

References

[1] E. Kandel, *et al*., "Principles of Neural Scienece," McGraw-Hill, 4th ed., 2000.

[2] J. Yu, M. Tan, J. Chen, and J. Zhang, "A Survey on CPG-Inspired Control Models and System Implementation," *IEEE Transactions on Neural Networks and Learning Systems*, Vol. 25, No.3, pp. 441–456, 2014.

[3] Y. J. Lee, J. Lee, K. K. Kim, Y. B. Kim, and J. Ayers, "Low power CMOS electronic central pattern generator design for a biomimetic underwater robot," *Neurocomputing*, Vol. 71, pp. 284–296, 2007.

[4] R. J. Kier, J. C. Ames, R. D. Beer, and R. R. Harrison, "Design and Implementation of Multipattern Generators in Analog VLSI," *IEEE Transactions on Neural Networks*, Vol. 17, No. 4, pp. 1025–1038, 2006.

[5] N. Sasagawa, K. Tani, T. Imamura, and Y. Maeda, "Quadruped Locomotion Patterns Generated by Desymmetrization of Symmetric Central Pattern Generator Hardware Network," IEICE Transactions on Fundamentals of Electronics, Communications and Computer Sciences, E101.A, No. 10, pp. 1658–1667, 2018.

[6] I. Köymen and E. M. Drakakis, "Current-input current-output analog half center oscillator and central pattern generator circuits with memristors," International Journal of Circuit Theory and Applications, Vol. 46, No. 7, pp. 1294–1310, 2018.

[7] F. Li, A. Basu, C. H. Chang, and A. H. Cohen, "Dynamical systems guided design and analysis of silicon oscillators for central pattern generators," IEEE transactions on circuits and systems I : regular papers, Vol. 59, No.12, pp. 3046–3059, 2012.

[8] R. J. Vogelstein, F. V. G. Tenore, L. Guevremont, R. Etienne-Cummings, and V. K. Mushahwar, "A Silicon Central Pattern Generator Controls Locomotion in Vivo," IEEE Transactions on Biomedical Circuits and Systems, Vol. 2, No. 3, pp. 212–222, 2008.

[9] H. Soleimani, A. Ahmadi, M. Bavandpour, and O. Sharifipoor, "A generalized analog implementation of piecewise linear neuron models using CCII building blocks," Neural Networks, Vol. 51, pp. 26–38, 2014.

[10] K. Nakada, T. Asai, and Y. Amemiya, "An Analog CMOS Central Pattern Generator for Interlimb Coodination in Quadruped Locomotion," *IEEE Transactions on Neural Networks*, Vol. 14, No. 5, pp. 1356–1365, 2003.

[11] W. Chen, G. Ren, J. Zhang, and J. Wang, "Smooth transition between different gaits of a hexapod robot via a central pattern generators algorithm," *Journal of Intelligent & Robotic Systems*, Vol. 67, No. 3–4, pp. 255–270, 2012.

[12] X. Li, H. Liu, X. Wu, R. Li, and X. Wang, "Improved CPG Model based on Hopf Oscillator for Gait Design of New Type of Hexapod Robot," Lecture Notes in Computer Science, Vol. 11741, pp. 72–83, 2019.

[13] B. Xu, W. Li, Y. Ni, H. Chi, and W. Ouyang, Adaptive Locomotion Generation for a Bionic Hexapod Robot. IECON 2019 - 45th Annual Conference of the IEEE Industrial Electronics Society. 5173–5178 (2019)

[14] B. Zhong, S. Zhang, M. Xu, Y. Zhou, T. Fang, and W. Li, "On a CPG-Based Hexapod Robot: AmphiHex-II With Variable Stiffness Legs," IEEE/ASME Transactions on Mechatronics, Vol. 23, No. 2, pp. 542–551, 2018.

[15] E. I. Guerra-Hernandez, A. Espinal, P. Batres-Mendoza, C. H. Garcia-Capulin, R. De J. Romero-Troncoso, and H. Rostro-Gonzalez, "A FPGA-Based Neuromorphic Locomotion System for Multi-Legged Robots," IEEE Access, Vol. 5, pp. 830–8312, 2017.

[16] A. Crespi and A. J. Ijspeert, "AmphiBot II: An Amphibious Snake Robot that Crawls and Swims using a Central Pattern Generator," *Proc. of the 9th International Conference on Climbing and Walking Robots*, pp. 19–27, 2006.

[17] A. Crespi, A. Badertscher, A. Guignard, and A. J. Ijspeert, "AmphiBot I: an amphibious snake-like robot," *Robotics and Autonomous Systems*, Vol. 50, No. 4, pp.163–175, 2005.

[18] L. Minati, M. Frasca, N. Yoshimura, and Y. Koike, "Versatile Locomotion Control of a Hexapod Robot Using a Hierarchical Network of Nonlinear Oscillator Circuits," IEEE Access, Vol. 6, pp. 8042–8065, 2018.

[19] C. Mayr, J. Partzsch, M. Noack, S. Hänzsche, S. Scholze, S. Höppner, G. Ellguth, and R. Schüffny, "A Biological-Realtime Neuromorphic System in 28 nm CMOS Using Low-Leakage Switched Capacitor Circuits," IEEE Transactions on Biomedical Circuits and Systems, Vol. 10, No. 1, pp. 243–254, 2016.

[20] N. Korkmaz, I. Ozuturk, and R. Kilic, "The investigation of chemical coupling in a HR neuron model with reconfigurable implementations," *Nonlinear Dynamics*, Vol. 86, pp. 1841–1854, 2016.

[21] Y. Maeda, T. Hiramatsu, S. Miyoshi, and H. Hikawa, "Pulse Coupled Oscillator with Learning Capability Using Simultaneous Perturbation and Its FPAA Implementation," *Proc. of the ICROS-SICE International Joint Conference 2009*, pp. 3142–3145, 2009.

[22] K. Takeda and H. Torikai, "A Novel Hardware-Efficient CPG Model based on Nonlinear Dynamics of Asynchronous Cellular Automaton," *Proc. of the 24th International Conference on Neural Information Processing*, Part III, Springer Lecture Notes in Computer Science 10639, pp. 812-820, 2017.

[23] K. Takeda and H. Torikai, "A Novel Hardware-Efficient CPG Model based on Asynchronous Cellular Automaton," *IEICE Electronics Express*, Vol. 15, No. 11, 20180387, 2018.

[24] K. Takeda and H. Torikai, "A novel hardware-efficient CPG model for a hexapod robot based on nonlinear dynamics of coupled asynchronous cellular automaton oscillators," *Proc. of the 2019 International Joint Conference on Neural Networks*, N-19758, 2019.

[25] K. Takeda and H. Torikai, "A Novel Asynchronous CA Neuron Model: Design of Neuron-like Nonlinear Responses based on Novel Bifurcation Theory of Asynchronous Sequential Logic Circuit," *IEEE Transactions on Circuit and Systems I: Regular Papers* (early access).

[26] D. M. Wilson, "Insect walking," Annual Review of Entomology, Vol. 11, pp. 103–122, 1966.

[27] Lynxmotion [Online]. Available: http://www.lynxmotion.com/

[28] Xilinx Inc., San Jose, CA [Online]. Available: http://www.xilinx.com/

[29] Digilent Inc. [Online]. Available: http://www.digilentinc.com/